Journal of Materials Chemistry A

Accepted Manuscript

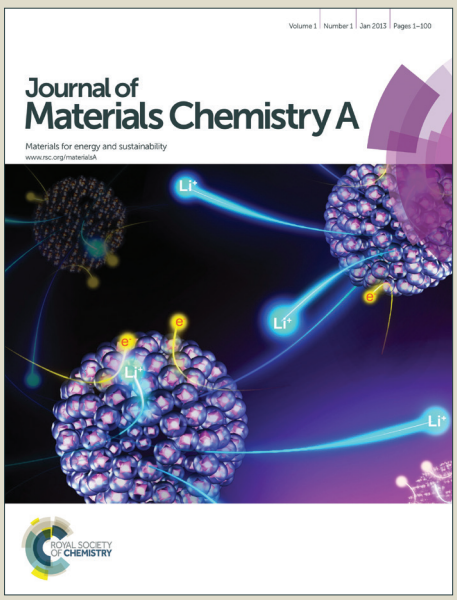

ROYAL SOCIETY OF CHEMISTRY

www.rsc.org/materialsA

Journal Name

RSCPublishing

ARTICLE

Monodisperse, ultrathin NiPt hollow nanospheres with tunable diameter and composition by a green chemical synthesis†

Cite this: DOI: 10.1039/xoxxoooooox

Received ooth January 2014,
Accepted ooth January 2014

DOI: 10.1039/xoxxoooooox

www.rsc.org/

Aixian Shan,[a,b] Zhichao Chen,[b] Bangquan Li,[a] Chinping Chen[b*] and Rongming Wang[a,c*]

Monodisperse NiPt hollow nanospheres with citric acid as surfactant were synthesized by a one-pot wet chemical method in water at room temperature. The diameter is adjustable from 13 to 100 nm with the shell thickness of 2-3 nm roughly the size of nanocrystallites. The composition is also tunable with the ratio of Ni:Pt from 1:9 to 9:1. A phase formation mechanism is proposed for the controllability of the diameter from the sacrificial templates of intermediate Ni-B amorphous nanocompounds. Molecular dynamic calculations show that 2 nm is the lower-bound shell thickness for a stable hollow spherical structure from distortion or collapse. The electrocatalytic properties for the oxidation of ethylene glycol are measured for the 35 nm $Ni_{50}Pt_{50}$ hollow nanospheres. Its performance is apparently better than that using commercial Pt/C catalyst. This makes it a potential application as fuel cells catalyst.

Key words: NiPt nanoalloy, ultrathin shell, bimetallic nanoparticle, hollow sphere, green synthesis, electrocatalysis.

Introduction

Recently alternative energy sources have attracted a lot of attentions.[1, 2] Particularly, methanol, ethanol, glycerol, and ethylene glycol (EG) have widespread applications in fuel cells, owing to their high volumetric energy density, energy efficiency, capacity, and recyclability.[3, 4] Among them, EG is one of the most promising candidates because of its lower toxicity, low volatility, and high volumetric energy density.[5] Platinum (Pt) is known as the best electrocatalyst in fuel cells to date.[6, 7] However, the large-scale industrial utilization of Pt catalyst with low cost, facile synthesis, high activity, and high stability still remains a challenge, which has restricted its commercialization.[8]

Bimetallic catalysts having core-shell[9, 10], heterostructure[11, 12], and intermetallic or alloyed structures[13-16] with distinctive electronic and chemical properties from their parent metals, offer the opportunity to obtain new catalysts with enhanced selectivity, activity, and stability.[1, 17] Especially, Pt-alloys involving 3d metals are better catalysts than the pure Pt because the electronic structure of the surface Pt atoms with the alloys has been slightly modified.[8, 18]

A number of works have been performed in tailoring the shape and size of Pt and Pt-based nanostructures to enhance the efficiency in catalysis by increasing the active surface area[19-23], including Pt nano-octahedrals[24], nano-icosahedrals[25], nano-wires[26], nano-tubes[27], nano-chains[28], nano-cubes[29], and hollow Pt nano-structures[22, 30-38] etc. Among them, hollow structures have several advantages such as low density, reduced cost, high surface area, improved utilization of the unit Pt, etc.[39]

Thus, it is highly desirable to synthesize bimetallic hollow structure Pt-based catalysts. In the present study, a green synthesis was carried out by a one-pot wet chemical method in water at room temperature. Nearly monodisperse hollow nanospheres of bimetallic NiPt were synthesized. The diameter was controllable from 13 to over 100 nm, as shown in Fig. S1 in ESI. The shell thickness reached down to about 2-3 nm. This is the thin shell limit for the structure stability without collapsing from a hollow sphere structure according to a molecular dynamic simulation study. The compositions were tunable for the ration of Ni:Pt from 9:1 to 1:9. The phase formation mechanisms are proposed. In particular, there are two routes for the size control, One is the commonly known method by adjusting the concentration of the Ni salt, while the other, interestingly, by changing the time duration for the reaction step causing the size variation of the intermediate sacrificial nanoparticles of Ni-B compounds. The catalytic properties for the EG oxidation reaction were studied. The primary oxidation peak in the cyclic voltammograms curve for the present NiPt nanospheres is 2.5 times more than that for the commercial Pt/C.

Experimental

$NiCl_2$ $6H_2O$ (nickel chloride hexahydrate), $NaBH_4$ (sodium borohydride), H_2PtCl_6 $6H_2O$ (chloroplatinic acid hexahydrate), $C_6H_8O_7$ (citric acid), were purchased from Chinese reagent companies. All reagents were analytic grade and used as received.

In a typical synthesis, 0.2 ml $NiCl_2$ aqueous solution (0.5 g in 10 ml Deionized (DI) water) and 8 mg $C_6H_8O_7$ was dissolved in 100 ml DI water. After the mixed solution was sonicated and protected in the argon for 15 min, a freshly prepared 13 mg $NaBH_4$ powder was then added quickly with vigorous stirring. The appearance of the black colour in the solution indicated that the intermediate compounds of Ni and B were produced. Then H_2PtCl_6 (20 ml 1 mM) was added dropwise immediately. Waiting for another 120 min, the product was collected by centrifugation and washed several times with ethanol.

The morphologies and chemical compositions of the as-synthesized products were characterized by X-ray diffractometry (XRD, X'Pert Pro MPD system, Cu Kα, λ = 0.154 nm), Imaging Photoelectron Spectrometer (XPS, Kratos Analytical Ltd. Axis Ultra), scanning electron microscopy (SEM, Hitachi S-4800) with an energy dispersive X-ray spectroscope (EDS), and transmission electron microscopy (TEM, JEOL 2100F at 200 kV). TEM samples were prepared by dispersing the powder in ethanol with ultrasonic treatment and then a solution was dropped on a Cu-grid coated with porous carbon film.

To prepare the working electrode for the electrolysis measurements, Pt catalyst (2 mg $Ni_{0.5}Pt_{0.5}$ and 5 mg Pt/C commercial catalyst) and 100 μL Nafion alcohol solution (5 wt %) were dispersed ultrasonically in 10 mL of DI water, and 3 μL of the suspension was pipetted onto a glassy carbon substrate (φ = 6 mm). The coated electrode was dried in air. The loading of platinum was about 1 μg cm^{-2}. Electrochemical experiments were carried out in a standard three-electrode cell at room temperature (about 25 ℃). The working electrode was a Pt wire and the reference electrode was a saturated calomel electrode (SCE). Electrode potential was controlled by a CHI 660C potentiostat/galvanostat.

Result and discussion

1 Characterization

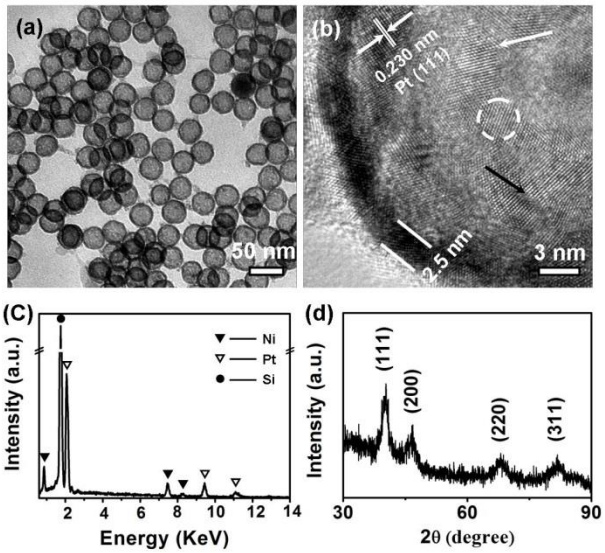

Fig. 1 (a) TEM image of the NiPt hollowspheres with a uniform diameter of about 35 nm; (b) A typical high-resolution TEM image of a part of a nanosphere. It shows the polycrystalline structure with a nano-crystallite size of about 3 nm; (c) EDS analysis revealing the atomic ratio of Ni : Pt as 1 : 1, (d) XRD pattern, indexed to Pt (JCPDS no. 87-0647).

The morphologies of the as-synthesized products were observed using TEM. Figure 1(a) shows an image for the nanospheres of about 35 nm in diameter with high uniformity in size and shell thickness. The shell is extremely thin about 2-3 nm as shown in figure 1(b), which presents a typical HRTEM (high-resolution TEM) image for a part of a nanosphere. The lattice fringes with a *d*-spacing of 0.230 nm correspond to the (111) planar distance of face-centered cubic (fcc) crystalline Pt. The nanospheres were formed with well-crystallized but randomly orientated nanocrystallites of a few nanometers (e.g. the one marked by the broken circle). Semi-coherent grain boundaries (marked by the white arrow) and amorphous grain boundaries (marked by a black arrow) are observed. Similar characteristics of crystallization have been observed and reported in the literature[33]. Figure 1(c) is an EDS spectrum of the sample acquired by a SEM, showing mainly Ni, Pt and Si characteristic peaks. Since the Si is from the supporting silicon wafer, we conclude that the as-synthesized samples contain only two elements, i.e., nickel and platinum. The atomic ratio is about 1:1. The powder XRD pattern of the as-synthesized material is recorded in figure 1(d). It exhibits a typical pattern of fcc lattice with a pure phase Pt. Significantly widened peak width and a slight deviation of peak position are attributed to the small-size effects and the alloying of Pt with Ni. By using the Debye-Scherer formula, $D = 0.89\,\lambda/(\beta\cos\theta_B)$, where λ is the X-ray wavelength (0.15406 nm), θ_B is the Bragg diffraction angle, and β is the peak width at half-maximum, the XRD peak of (111) in figure 1(d) gives an average particle size of ~ 3 nm. It is in accordance with that obtained from the HRTEM image shown in Figure 1(b). We conclude that the shell thickness of 2~3 nm is about the size of a single nano-crystallite.

2 Phase formation

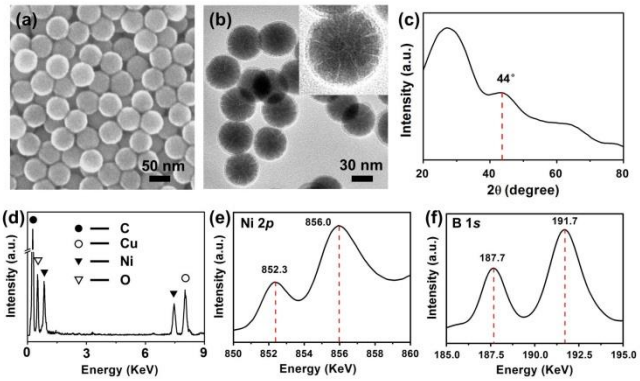

Fig. 2 (a) SEM image; (b) TEM image; (c) XRD pattern for the intermediate nanoparticles of amorphous Ni-B compound; In Fig. 2(c), the broad peak centered at $2\theta = 44°$ is a characteristic feature for the Ni-B amorphous alloy structure; (d) EDS analysis of the same Ni-B compounds; (e) XPS analysis of Ni 2*p*. The peak at 852.3 eV can be assigned to metallic Ni, while 856.0 eV, to oxidized Ni. (f) XPS analysis of B 1*s*. The peak at 187.7 eV is for the elemental B, while 197.7 eV, for the oxidized B.

Figure 2 demonstrates that Ni-B compounds in uniform size are formed as an intermediate in the reaction processes towards the final product. The Ni-B compounds contain both of the elemental Ni and B, when Ni ions are fast reduced by $NaBH_4$. They are monodisperse with a diameter around 50 nm as shown in figures 2(a) and (b) by SEM and TEM images, respectively. In fact, the diameter depends on the raw material concentration of nickel chloride along with the time window to add the chloroplatinic acid solution. Their role as a sacrificial template in controlling the diameter of the final products of hollow spheres will be elaborated later. Cracking structures are clearly observed in the inset of figure 2(b). The XRD patterns in figure 2(c) indicate that these nanoparticles are amorphous. The broad peak centered at 2θ, about 45 °, is a characteristic feature for the Ni-B amorphous compound[40]. The EDS spectrum, acquired by the TEM, shows the C, Ni, O and Cu characteristic peaks. Knowing that C and Cu originate from the supporting Cu-grid with an amorphous carbon film, we conclude that the intermediate Ni-B compounds indeed contains the Ni elements. Despite evidences for its presence by XRD in Fig. 2(c) and by XPS presented later in Figure 2(f), the B element is not revealed by EDS due to the sensitivity of the instrument. There might be O element also in the compounds, because oxygen exists in the reaction solution inevitably and Ni is easily oxidized. The surface electronic states and the chemical bonding between Ni and B in the sample are determined by XPS as shown in figures 2(e) and (f). The characteristic peaks of Ni 2*p* centered at 852.3 eV and 856.0 eV can be assigned to metallic and oxidized Ni, respectively[41]. The B species are present in both of the elemental and the oxidized forms, with B 1*s* binding energy (BE) values of around 187.7 and 197.7 eV, respectively. The B 1*s* BE of the elemental B in the sample exceeded that of pure B (187.1 eV)[42] by 0.6 eV, indicating that the elemental B is alloyed with the metallic Ni. Meanwhile, when $NaBH_4$ powder dissolves in water, it is easily hydrolyzed.

So, the intermediate nanoparticles of Ni-B compounds are formed by adding the $NaBH_4$ powder in to the solution of Ni salt. After the initial reaction taking place for several minutes, aqueous solution of chloroplatinic acid is added. As the standard reduction potential of Ni^{2+}/Ni (E^0 = -0.25 eV *vs*. SHE) is lower than that of the $PtCl_6^{2-}/Pt$ pair (E^0 = 0.75 eV *vs*. SHE), once the chloroplatinic acid is added, the galvanic replacement would occur immediately. The Pt ions would be reduced to metallic Pt at the expense of Ni in the Ni-B amorphous compounds, and described by Eq. (1). In the meanwhile, the Ni ions would be co-reduced with $PtCl_6^{2-}$ at the presence of excessive $NaBH_4$, as described by Eqs. (2) and (3). This leads to the formation of NiPt alloying nanostructures. The composition ratio of Ni over Pt is thus adjustable depending on the amount and concentration of the initial reactants.[43, 44] In the reaction, the intermediate nanoparticles of Ni-B compounds actually acts as sacrificial templates for the formation of hollow sphere structures, by providing the Ni to alloy with Pt. In this sense, the diameter of the hollow nanospheres are tunable depending on the diameter of the intermediate Ni-B nano-compounds, which, in turn, is adjustable via a well-known corrosion process of metallic Ni by the Cl^- ions in the solution. The evidences of size control for the intermediate sacrificial Ni-B nano-compounds will be presented later in this paper.

$$2Ni + PtCl_6^{2-} = 2Ni^{2+} + Pt\downarrow + 6Cl^- \quad (1)$$

$$BH_4^- + 4Ni^{2+} + 8OH^- = 4Ni\downarrow + BO_2^- + 6H_2O \quad (2)$$

$$2PtCl_6^{2-} + BH_4^- + 8OH^- = 2Pt\downarrow + BO_2^- + 6H_2O + 12Cl^- \quad (3)$$

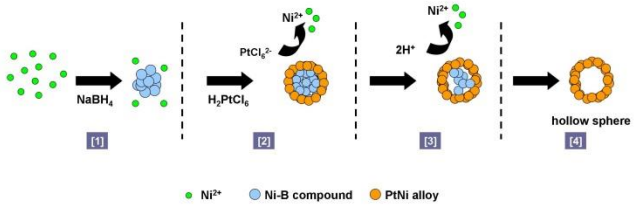

Fig. 3 Schematic illustration for the formation of NiPt hollow nanoparticles. The Ni based intermediate nanoparticles appear first in step (1). Hollow nanoparticles of NiPt were obtained in Step (4) with Ni-B compounds as a sacrifice template depicted in steps (2) and (3).

A schematic illustration for the formation of the NiPt hollow nanoparticles is presented in figure 3. At first, Ni ions are fast reduced by $NaBH_4$ to form nanoparticles of amorphous Ni-B nano-compounds, depicted in step (1) of Fig. 3. After chloroplatinic acid is added, Pt ions are reduced at the expense of the Ni in the Ni-B compounds. Then, Pt along with the co-reduced Ni forms NiPt nano-crystallite over the surface the Ni-B compounds, described in step (2). With the additional acid corrosion effects on the Ni-B nano-compounds, NiPt hollow alloys are formed, step (3) and (4). Recently, Erlebacher et al. have proposed a possible mechanism other than the slow Kirkendall mechanism for the fast formation of hollow nanoparticle based on a sacrificial template. They find that there is typically enough thermal energy at room temperature to result in a sufficiently large fluctuation in the shell thickness, so that the cores might be transiently exposed to the surrounding acidic environment and dissolves away. Then a hollow shell

containing a pinhole is formed, which would quickly close to eventually leave a hollow nanoparticle.[45]

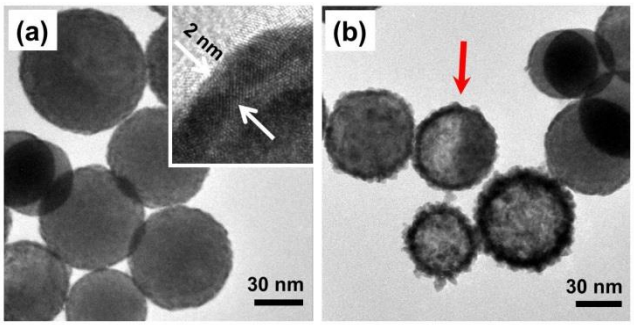

Fig. 4 TEM images for the NiPt products (a) with core-shell structures when the addition of low concentration H_2PtCl_6 solution, only 40% the regular value for a complete hollow structure. The inset is an HRTEM image showing that some of the inner core is indeed reacted away. (b) Partially hollow structures are obtained with a higher concentration, about 60% the regular value of H_2PtCl_6 solution.

As shown in Fig. 4, when the H_2PtCl_6 with low concentration was added, about 40% and 60% of the concentration needed to form hollow structures, there will be core-shell (Fig. 4(a)) or semi-hollow (Fig. 4(b)) structure in the NiPt products. The shell thickness is about 2 nm in the NiPt core-shell nanospheres, and the lattice fringe of Pt is clear in the HRTEM image of the inset in Fig 4(a). Some of the inner core is even consumed away by reaction, indicating the onset of the sacrificial processes. It is corresponding to the step (2) in Fig. (3). From Fig. 4(b), the hollow spheres coexist with the core-shell structure, meanwhile, semi-hollow sphere, which is pointed by an arrow, is found. It is corresponding to the step (3) in Fig. (3)

3 Size control

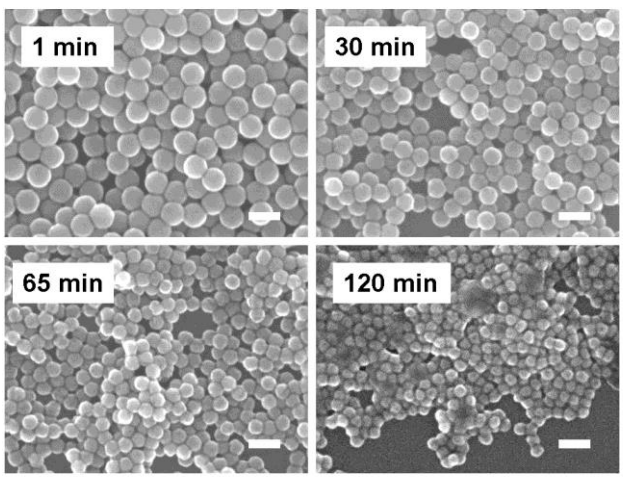

Fig. 5 SEM images for the sacrificial template of Ni-B nano-compounds. The size decreases with the increasing reaction time. The scale bars are all of 100 nm.

The diameters of the hollow NiPt nanospheres are adjustable usually via two different routes. One is by changing the concentration of reactants[33]. Another is by controlling the amount of surfactant[38]. In this paper, a third mechanism is proposed. The size of the sacrificial nanoparticles of Ni-B compounds depends on the reaction time before the aqueous solution of chloroplatinic acid is added, as depicted by step (1) of Fig. 3. This is possibly due to the slow corrosion effects on the metallic Ni by the Cl ions in the solution. The SEM images in Fig. 5 and Fig. S2 in ESI reveal that the size of the sacrificial nanoparticles reduces with the reaction time progressively. The diameters of the NiPt hollow spheres are thus adjustable accordingly, as revealed in Fig. S1 in ESI. The composition is also adjustable with the ratio of Ni:Pt from 1:9 to 9:1 , presented in a previous paper.[46]

4 Structural stability

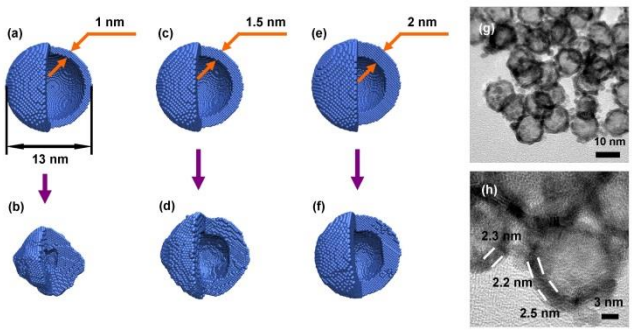

Fig. 6 Structural stability of hollow spheres depending on the shell thickness. Molecular dynamic simulation for an initial spherical hollow structure of fcc Pt crystal with 13 nm in outer diameter and (a) 1 nm, (c) 1.5 nm, (e) 2 nm in shell thickness. After a time evolution the final equilibrium structures are presented in (b), (d) and (f) corresponding to (a), (c) and (e) respectively. It indicates that the minimum shell thickness is 2 nm to have a spherical shape of hollow structure. (g) TEM and (h) HRTEM image of uniform Pt-rich, with atomic ratio of 9:1 for Pt:Ni, These NiPt hollow nanospheres are about 13 nm in outer diameter and 2 nm in shell thickness.

There is a thin limit in the shell thickness for the formation of a spherical hollow structure. Molecular dynamics (MD) simulations have been performed for Au to investigate this effect in the literature[47]. We adopt the same method to calculate hollow nanoparticles of pure Pt with 13 nm in outer diameter and 1, 1.5 and 2 nm in shell thickness. A time step of 1.2 fs is used for all MD simulations. The temperature of the system is kept constant at 300 K during the whole process with a velocity rescaling method. The interaction between Pt atoms is described by the potential proposed by Zhou *et al*.[48] We take pure Pt hollow nanospheres to simplify the calculation for the experimental Pt-rich hollow nanospheres of the same size with the atomic ratio of 9:1 for Pt over Ni. For the shell thickness of 1 nm, the calculation gives a collapsing structure, Fig. 6(b), from an initial spherical one, Fig. 6(a). For the shell thickness of 1.5 nm, the initial spherical structure, Fig. 6(c), would evolve into a distorted structure, Fig. 6(d). The experimental results in Fig. 6(g) by TEM and Fig. 6(h) by HRTEM show that the Pt-rich hollow nanospheres of 13 nm in outer diameter have a shell thickness of about 2 nm, which is about the smallest value for a stable spherical structure according to the MD simulation.

5. Catalysis

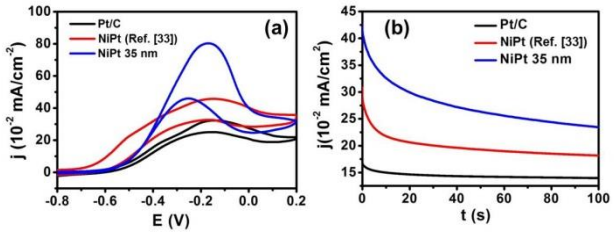

Fig. 7 (a) Cyclic voltammograms and (b) chronoamperometric curves at 0.15 V on 35 nm NiPt hollow spheres (blue), NiPt hollow spheres synthetized according to Ref. [33] (red) and commercial Pt/C (black) in 1.0 M potassium hydroxide (KOH) solution containing 1 M ethylene glycol ($C_2H_6O_2$).

Three samples were tested in the electrocatalytic experiment, namely, 35 nm NiPt hollow nanoparticles synthesized in the present work, NiPt hollow spheres synthesized with polyvinyl pyrrolidone (PVP) as the surfactant according to Ref. [33] and commercial Pt/C. The electrochemically active surface area (ECSA) is not only associated with the number of active sites available, but also includes the access of a conductive path to transfer the electrons to and from the electrode surface.[49] Hydrogen adsorption/ desorption peaks are usually used to evaluate ECSA of a catalyst. Fig. S3 in ESI shows the cycilc voltammograms of 35 nm NiPt hollow sphere, NiPt hollow sphere coated by PVP[33] and commercial Pt/C in N_2-saturated 0.5 M H_2SO_4 at a scan rate of 50 mV s^{-1}. They show characteristic peaks for the formation and reduction of Pt oxide. In the potential region of -0.2 V to 0 V, we observe the typical hydrogen adsorption and desorption peaks from polycrystalline Pt. It is estimated to be 141.9 m^2g^{-1} Pt on the 35 nm NiPt hollow sphere, which is much larger than that of commercial Pt/C with a value of 78.3 m^2g^{-1} Pt and the value of 94.3 m^2g^{-1} Pt for the NiPt hollow sphere coated by PVP[33]. These results demonstrate the improved performance of the NiPt hollow sphere.

The electrocatalytic activity of these three samples in the oxidation of ethylene glycol (EG) was tested in the 1 M KOH and 1 M C_2H_6O between -0.8 V and 0.2 V at the sweep rate of 50 mV s^{-1}. As shown in figure 7(a), during the positive scan, the current increases until a higher peak is seen at -0.15 V, which is attributed to the complete electro-oxidation of EG. While the lower peak at -0.25 V in the negative sweep is associated with the removal of incompletely oxidized carbonaceous species. The 35 nm NiPt hollow nanoparticles showed the highest forward current density (0.8 mA cm^{-2}), which is 1.7 and 2.7 times higher than NiPt hollow spheres coated with PVP[33] and commercial Pt/C, respectively.

The electrocatalytic activity and stability of these three samples were further compared by using chronoamperometry test at 0.15 V. The oxidation current density with the 35 nm hollow NiPt nanospheres is higher than with the NiPt hollow spheres coated with PVP[33] and Pt/C catalyst. This result along with the cyclic voltammetry measurements confirms that the electrocatalytic activity and stability of the 35 nm hollow NiPt catalysts are the highest among the three samples under study.

The much enhanced catalytic activity for the EG oxidation may be attributed to the increasing specific surface, arising from the additional active sites provided by the inner surface of the NiPt hollow nanospheres[39, 50]. For the synthesized 35 nm hollow spheres, the porosity of the surface is clearly observed in TEM image (Fig. S4 in ESI). The increase of active sites for the synthesized sample is shown in ECSA measurement (Fig. S3 in ESI).

Conclusions

In summary, nearly monodisperse hollow nanospheres of bimetallic NiPt were synthesized by a one-pot, green, wet chemical method at room temperature. The diameter is tunable from 13 to 100 nm with the shell thickness of about 2 to 3 nm. Numerical simulations by molecular dynamic calculations indicate that the minimum shell thickness is about 2 nm for a stable hollow structure of 13 nm in diameter. A phase formation mechanism by the sacrificial template of intermediate Ni-B compounds is proposed for the size control. The composition ratio of Ni over Pt is adjustable as well, from 1:9 to 9:1. The synthesized hollow NiPt nanospheres exhibit considerably enhanced catalytic activities for the oxidation of ethylene glycol compared to commercial Pt/C catalysts and hollow NiPt catalysts synthesized with PVP as surfactant. It is a promising candidate as catalysts and sensing materials for the ease of synthesis, low cost, environmental friendly and excellent electrocatalytic activity.

Acknowledgements

This work was supported by the National Natural Science Foundation of China (no.11174023, 51371015, 51331002), Beijing Natural Science Foundation (no.2142018) and the Fundamental Research Funds for the Central Universities.

Notes and references

[a] Department of Physics, BeiHang University, Beijing 100191, China;
[b] Department of Physics, Peking University, Beijing 100871, China;
[c] School of Mathematics and Physics, University of Science and Technology Beijing, Beijing 100083, PR China;
* To whom correspondence should be addressed.
E-mail: cpchen@pku.edu.cn; rmwang@ustb.edu.cn

† Electronic supplementary information (ESI) available: **Fig. S1** shows the TEM pictures of the synthesized hollow spheres with different diameters. **Fig. S2** shows the SEM images for the sacrificial template of Ni-B nano-compounds. The size decreases with the increasing reaction time. **Figure S3** shows the cyclic voltammograms for 35 nm NiPt hollow sphere, NiPt hollow sphere coated by PVP (Ref.[33]) and Pt/C in N_2-saturated 0.5 M H_2SO_4 at a scan rate of 50 mV s^{-1}. **Fig. S4** shows the detailed TEM picture of the porosity of the surface for hollow NiPt nanospheres.

1. A. K. Singh and Q. Xu, *Chemcatchem*, 2013, **5**, 652-676.
2. U. A. Icardi, S. Specchia, G. J. R. Fontana, G. Saracco and V. Specchia, *J Power Sources*, 2008, **176**, 460-467.
3. H. R. Yue, Y. J. Zhao, X. B. Ma and J. L. Gong, *Chem Soc Rev*, 2012, **41**, 4218-4244.

4. J. M. Sieben and M. M. E. Duarte, *Int J Hydrogen Energ*, 2012, **37**, 9941-9947.
5. J. N. Zheng, J. J. Lv, S. S. Li, M. W. Xue, A. J. Wang and J. J. Feng, *J Mater Chem A*, 2014, **2**, 3445-3451.
6. M. K. Debe, *Nature*, 2012, **486**, 43-51.
7. A. Rabis, P. Rodriguez and T. J. Schmidt, *Acs Catal*, 2012, **2**, 864-890.
8. Y. H. Bing, H. S. Liu, L. Zhang, D. Ghosh and J. J. Zhang, *Chem Soc Rev*, 2010, **39**, 2184-2202.
9. Y. C. Hsieh, Y. Zhang, D. Su, V. Volkov, R. Si, L. J. Wu, Y. M. Zhu, W. An, P. Liu, P. He, S. Y. Ye, R. R. Adzic and J. X. Wang, *Nat Commun*, 2013, **4**, 2466.
10. D. Amara and S. Margel, *J Mater Chem*, 2012, **22**, 9268-9276.
11. X. W. Liu, W. Y. Wang, H. Li, L. S. Li, G. B. Zhou, R. Yu, D. S. Wang and Y. D. Li, *Sci Rep-Uk*, 2013, **3**, 1404.
12. D. L. Wang, H. L. L. Xin, R. Hovden, H. S. Wang, Y. C. Yu, D. A. Muller, F. J. DiSalvo and H. D. Abruna, *Nat Mater*, 2013, **12**, 81-87.
13. J. B. Wu, J. L. Zhang, Z. M. Peng, S. C. Yang, F. T. Wagner and H. Yang, *J Am Chem Soc*, 2010, **132**, 4984-4985.
14. C. H. Cui, L. Gan, M. Heggen, S. Rudi and P. Strasser, *Nat Mater*, 2013, **12**, 765-771.
15. S. I. Choi, S. F. Xie, M. H. Shao, J. H. Odell, N. Lu, H. C. Peng, L. Protsailo, S. Guerrero, J. H. Park, X. H. Xia, J. G. Wang, M. J. Kim and Y. N. Xia, *Nano Lett*, 2013, **13**, 3420-3425.
16. J. Zhang, H. Z. Yang, J. Y. Fang and S. Z. Zou, *Nano Lett*, 2010, **10**, 638-644.
17. S. B. Duan and R. M. Wang, *Prog Nat Sci-Mater*, 2013, **23**, 113-126.
18. J. K. Norskov, T. Bligaard, B. Hvolbaek, F. Abild-Pedersen, I. Chorkendorff and C. H. Christensen, *Chem Soc Rev*, 2008, **37**, 2163-2171.
19. J. W. Hong, S. W. Kang, B. S. Choi, D. Kim, S. B. Lee and S. W. Han, *Acs Nano*, 2012, **6**, 2410-2419.
20. C. Koenigsmann, W. P. Zhou, R. R. Adzic, E. Sutter and S. S. Wong, *Nano Lett*, 2010, **10**, 2806-2811.
21. C. Wang, H. Daimon, T. Onodera, T. Koda and S. H. Sun, *Angew Chem Int Edit*, 2008, **47**, 3588-3591.
22. J. X. Wang, C. Ma, Y. M. Choi, D. Su, Y. M. Zhu, P. Liu, R. Si, M. B. Vukmirovic, Y. Zhang and R. R. Adzic, *J Am Chem Soc*, 2011, **133**, 13551-13557.
23. H. Ataee-Esfahani, Y. Nemoto, L. Wang and Y. Yamauchi, *Chem Commun*, 2011, **47**, 3885-3887.
24. J. B. Wu, A. Gross and H. Yang, *Nano Lett*, 2011, **11**, 798-802.
25. W. Zhou, J. B. Wu and H. Yang, *Nano Lett*, 2013, **13**, 2870-2874.
26. Y. X. Li, Q. Q. Wu, S. F. Jiao, C. D. Xu and L. Wang, *Anal Chem*, 2013, **85**, 4135-4140.
27. Y. Kim, H. J. Kim, Y. S. Kim, S. M. Choi, M. H. Seo and W. B. Kim, *J Phys Chem C*, 2012, **116**, 18093-18100.
28. Q. Sun, S. G. Wang and R. M. Wang, *J Phys Chem C*, 2012, **116**, 5352-5357.
29. S. B. Han, Y. J. Song, J. M. Lee, J. Y. Kim and K. W. Park, *Electrochem Commun*, 2008, **10**, 1044-1047.
30. Y. P. Xiao, S. Wan, X. Zhang, J. S. Hu, Z. D. Wei and L. J. Wan, *Chem Commun*, 2012, **48**, 10331-10333.
31. H. P. Liang, H. M. Zhang, J. S. Hu, Y. G. Guo, L. J. Wan and C. L. Bai, *Angew Chem Int Edit*, 2004, **43**, 1540-1543.
32. S. J. Kim, C. S. Ah and D. J. Jang, *Adv Mater*, 2007, **19**, 1064-1068.
33. Q. Sun, Z. Ren, R. M. Wang, N. Wang and X. Cao, *J Mater Chem*, 2011, **21**, 1925-1930.
34. M. Xue and Y. Tan, *Nanoscale*, 2014, **6**, 12500-12514.
35. M. Y. Yang, Q. X. Cai, C. Liu, R. Wu, D. M. Sun, Y. Chen, Y. W. Tang and T. H. Lu, *J Mater Chem A*, 2014, **2**, 13738-13743.
36. Y. Xiao, Q. Lv, J. B. Zhu, S. K. Yao, C. P. Liu and W. Xing, *Rsc Adv*, 2014, **4**, 21176-21179.
37. Y. Feng, H. Liu, P. F. Wang, F. Ye, Q. Q. Tan and J. Yang, *Sci Rep-Uk*, 2014, **4**, 6204.
38. H. Li, H. Lin, Y. Hu, H. X. Li, P. Li and X. G. Zhou, *J Mater Chem*, 2011, **21**, 18447-18453.
39. X. W. Zhou, Y. L. Gan, J. J. Du, D. N. Tian, R. H. Zhang, C. Y. Yang and Z. X. Dai, *J Power Sources*, 2013, **232**, 310-322.
40. H. Li, Y. Xu, J. Liu, Q. F. Zhao and H. X. Li, *J Colloid Interf Sci*, 2009, **334**, 176-182.
41. G. Y. Bai, Z. Zhao, L. B. Niu, H. X. Dong, M. D. Qiu, F. Li, Q. Z. Chen and G. F. Chen, *Catal Commun*, 2012, **23**, 34-38.
42. J. Q. Ma, L. Xu, L. Xu, H. Wang, S. Xu, H. X. Li, S. H. Xie and H. Li, *Acs Catal*, 2013, **3**, 985-992.
43. M. Wang, W. M. Zhang, J. Z. Wang, A. Minett, V. Lo, H. K. Liu and J. Chen, *J Mater Chem A*, 2013, **1**, 2391-2394.
44. Y. Vasquez, A. K. Sra and R. E. Schaak, *J Am Chem Soc*, 2005, **127**, 12504-12505.
45. J. Erlebacher and D. Margetis, *Phys Rev Lett*, 2014, **112**.
46. A. X. Shan, M. Cheng, H. S. Fan, Z. C. Chen, R. M. Wang and C. P. Chen, *Prog Nat Sci-Mater*, 2014, **24**, 175-178.
47. L. Y. Jiang, X. Yin, J. W. Zhao, H. M. Liu, Y. H. Liu, F. Y. Wang, J. J. Zhu, F. Boey and H. Zhang, *J Phys Chem C*, 2009, **113**, 20193-20197.
48. X. W. Zhou, R. A. Johnson and H. N. G. Wadley, *Phys Rev B*, 2004, **69**, 14413.
49. Y. J. Hu, P. Wu, H. Zhang and C. X. Cai, *Electrochim Acta*, 2012, **85**, 314-321.
50. W. Q. Zhang, J. Z. Yang and X. M. Lu, *Acs Nano*, 2012, **6**, 7397-7405.

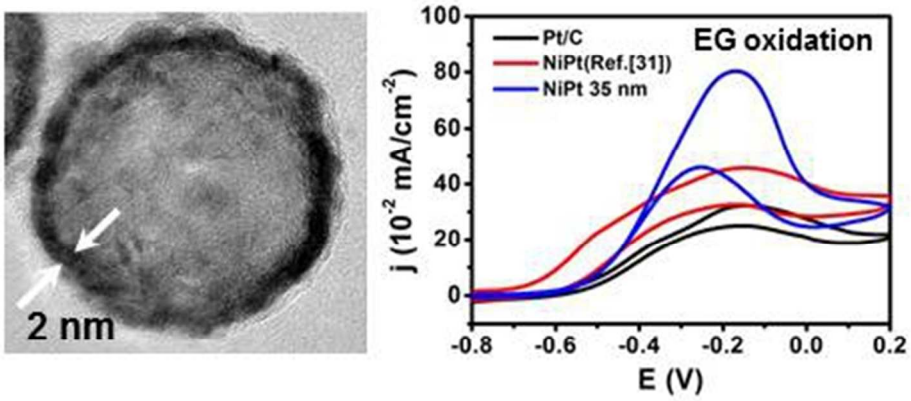

Monodisperse NiPt hollow nanospheres with tunable sizes were synthesized by a green chemical synthesis, which have excellent electrocatalytic properties.
79x39mm (150 x 150 DPI)